Nanoclays Dispersion in a PA6/PP Blend by Twin Screw Compounding

J. A. Covas,[*1] *M. F. Almeida,*[1] *A. V. Machado,*[1] *N. M. Larocca,*[2] *L. A. Pessan*[2]

Summary: A modified PP and an organoclay (Cloisite C15A, a montmorillonite modified with alkyl ammonium) were incorporated in a PA/PP 70/30 w/w blend by means of twin-screw melt compounding. The dispersion of the nanoclay into the polymer matrix and its eventual compatibilization effect were investigated by collecting samples along the barrel and characterizing them by X-ray diffraction (XRD), oscillatory rheometry, scanning and transmission microscopy (SEM and TEM). Chemical and morphological changes occurred mostly during polymer melting. The morphologies of the nanocomposite and of the compatibilized blends were much finer than that of the physical blend. When both the modified PP and the organoclay were present the morphology was even finer, suggesting that the organoclays may produce a compatibilization effect similar to that of PP-g-MA.

Keywords: blending; compatibilization; compounding; nanocomposites; organoclay

Introduction

Since it was observed that the dispersion of an organoclay in a polymer could result in final excellent mechanical and physical properties, along with good processability,[1–4] nanocomposites gained wide interest for both industry and academia. Organically modified Montmorillonite (OMMT modified) are probably the most popular. Also, melt compounding is often used, given its easy scale-up to industrial production, and capacity to generate the hydrodynamic stresses required for clay intercalation and exfoliation.[5,6]

Although the effect of dispersing organoclays in polymer blends has been reported,[3,4,7–11] fundamental questions concerning their eventual compatibilization effect, or the evolution of dispersion along the screw axis, are still to be answered. For example, while the decrease of the particle size of the dispersed phase usually associated to the presence of organoclays is generally attributed to a compatibilization effect of the organoclay,[7–11] some authors explained it by the lamellar and fibrilar forms of the blend phases in the presence of organoclays.[12] Reports on the evolution of dispersion along the screw are scarcer. Lertwimolnun and Vergnes[13] reported that intercalation is a rapid mechanism that occurs rapidly in the screw.

Thus, aiming to obtain information on nanoclays dispersion in a PA/PP blends during extrusion, a PA6/PP blend was compounded with PP-g-MA and OMMT to generate PA6/PP/OMMT and PA6/PP/PP-g-MA/OMMT nanocomposites. Samples collected along the barrel and extrudates were characterized by XRD, rheometry, SEM and TEM, in order to monitor, either directly or indirectly, the evolution of morphology along the process and better understand the associated compatibilization effects.

Materials and Experimental Procedure

A polyamide 6, PA6 (DOMAMID 27 from Atofina, with MFI value between 17

[1] I3N-Institute of Nanostructure, Nanomodelling and Nanofabrication University of Minho, Guimarães, Portugal
E-mail: jcovas@dep.uminho.pt
[2] Federal University of São Carlos, Dept Mat Sci Eng, São Carlos, SP, Brazil

Table 1.
PA6/PP blends and MMT nanocomposites produced.

Blends	PA6 (wt%)	PP (wt%)	PP-g-MA (phr)	C15A (phr)
PA6/PP	70	30	0	0
PA6/PP/C15A	70	30	0	5
PA6/PP/PP-g-MA/C 15 A	70	30	5	5

and 23 g/10 min, at 235°C and 2.16 kg), and a polypropylene homopolymer, PP, (MOPLEN - HP502N from Basell, with MFI value of 12 g/10 min at 230 °C and 2.16 kg) were used as the components of the immiscible blend. The compatibilizer, a PP grafted with maleic anhydride containing 1 wt. % MA, was obtained from Arkema (Orevac CA 100, with a MFI of 150 g/10 min at 230 °C and 2.16 kg). The organoclay selected (Cloisite 15A), a montmorillonite modified organically with 125 meq/100 g of quaternary alkylammonium salts, was produced by Southern Clay Products.

Table 1 shows the various blends and nanocomposites that were prepared in a Leistritz LSM 30.34 intermeshing co-rotating twin screw extruder (TSE) under fixed operating conditions (barrel and die set uniformly at 230 °C, screws rotating at 200 rpm and a feed rate of 4 kg/h imposed by a K-Tron gravimetric feeder). Melt compounding was preceded by drying the PA6 and the nanoclay under vacuum at 80 °C during 12–16 hours, and then tumble-mixing with PP or PP-g-MA, in order to obtain the compositions PA6/PP 70/30 w/w, PA6/PP/C15A 70/30/5 w/w/w and PA6/PP/PP-g-MA/C15A 70/30/5/5 w/w/w/w.

The extruder layout, screw configuration and axial location of the sample collecting devices are illustrated in Figure 1. The screws are 29D long and contain four mixing zones separated by feeding elements. As the material progresses towards the die, it must flow along 12 kneading disks plus a left-handed element, four kneading disks, three kneading disks and a left hand element, respectively. These kneading blocks are staggered negatively (−30°). Such a high shear screw profile was believed to be adequate to ensure the necessary dispersion levels. The barrel was fitted with a number of sample collecting devices, which enable the removal of material samples from inside the extruder in approximately 1 second. These samples are then immediately quenched in liquid nitrogen for subsequent characterization. The devices are located in regions where positive pressure develops, not only because sample collection is quicker, but also because one would anticipate that chemical or morphological evolutions should develop more significantly. Thus, the experimental procedure followed the scheme of Figure 2.

XRD spectra of the samples were obtained using a Rigaku Geigerflex dif-

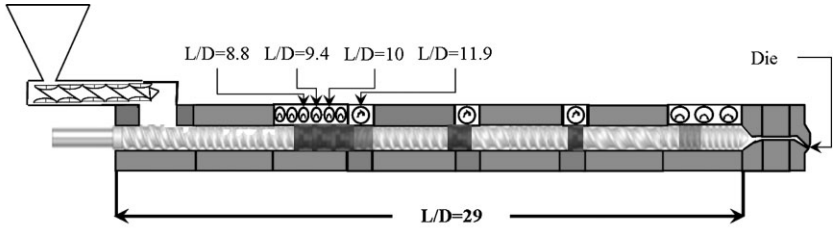

Co-rotating twin screw extruder, TSE (Leistritz LSM 30.34)

Screw Configuration:

45R/30R/30R2/12KD-30°/30R4L/30R/4KD-30°/45R2/30R2/30R4/3KD-30°/60R/20R4L/30R4/20R2

Figure 1.
Extruder layout, screw configuration and location of material sampling devices.

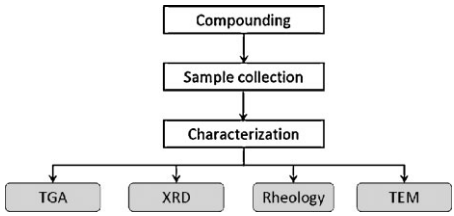

Figure 2.
Experimental procedure.

fractometer operating with CuKα radiation at 40 Kv and 25 mA, with a wavelength of 1.54 Å, the 2θ Bragg angles being varied from 1.7° to 5°.

Samples were also compression moulded into disks (under a pressure of 30 ton for 10 minutes at 230 °C) and then subjected to isothermal frequency sweeps from 0.01 to 100 Hz, at 230 °C, in a TA instruments RG2 oscillatory rheometer, working with a parallel-plate geometry (diameter 25 mm, gap of 0.9 mm). The strain was kept at 1% to guarantee a linear viscoelastic response.

The morphology of the blends and nanocomposites was analyzed with a Leica Cambridge S 360 Scanning Electron Microscope (SEM), after fracturing the samples in liquid nitrogen and etching them with hot xylene to remove the PP. At least 200 particles of the dispersed phase were taken into consideration when estimating their average particle with the *Image Pro.plus 4.5* software. Some samples were also analyzed by Transmission Electron Mocroscopy, TEM (Zeiss 902A, operating with a voltage of 80 kV). Slices of the samples with a thickness smaller than 90 nm were obtained by cryo-ultramicrotomy (at −45 °C, under liquid nitrogen), using a diamond knife and then stained with RuO_4 vapor for 6 hours at room temperature.

Results and Discussion

Extrudates

Figure 3 compares the XRD spectra and the rheological response of the original materials and nanocomposites at the die exit. Figure 3a shows the XRD spectra of the Cloisite 15A and of the two nanocomposites prepared (PA6/PP/C15A and PA6/PP/PP-g-MA/C15A), the latter being virtually matching. The peak of the organophilic clay at 2.76° (corresponding to a basal spacing of 31.9 Å, as given by Bragg's law[14]) is shifted in the nanocomposites to a lower angle (2.41°), which corresponds to an increase of the interplanar spacing of the organoclay layers to circa 36.6 Å. This can be interpreted as evidence of the formation of an intercalated structure.[15] In addition, the existence of a broader characteristic peak can also be explained by the development of some exfoliation.[16]

The rheological behavior presented in Figure 3b (in terms of the complex

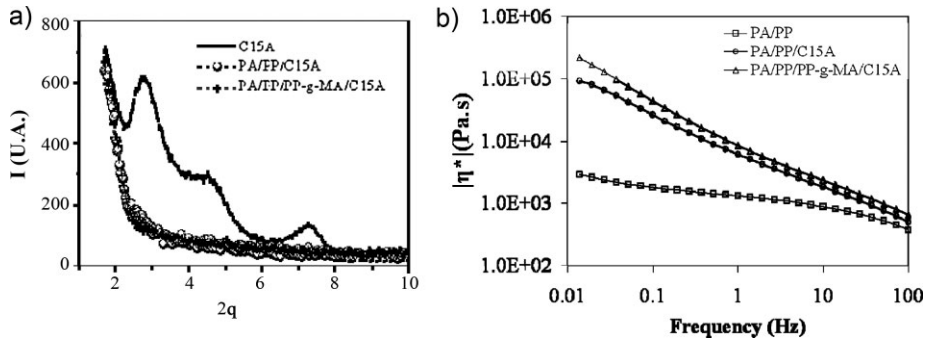

Figure 3.
XRD spectra (a) and complex viscosity (b) of the initial materials and nanocomposites (PA6/PP/C15A and PA6/PP/PP-g-MA/C15A).

viscosity, η^*) is consistent previous reports,[13,16] i.e., the incorporation of the clay particles (PA6/PP/C15A) increases significantly the magnitude of the complex viscosity, especially at low frequencies (a similar behavior takes place with the storage and loss moduli). At constant organoclay content, viscosity levels increase with higher dispersion levels. The presence of the modified PP (PA6/PP/PP-g-MA/C15A) induces a further raise in viscosity. Since the viscosity of the modified PP is much lower than that of the PP homopolymer (see values of their MFIs), this additional increase must be explained by a higher interphase and/or a lower average size of the dispersed phase, which are usually the result of a compatibilization effect.

The data in Figure 3 seem to indicate that good dispersion levels were obtained with the technology (melt compounding) processing conditions utilized. Nevertheless, an estimation of the average size of the dispersed phase from SEM micrographs is given in Figure 4. Figure 4a shows, from top to bottom, the morphologies of the immiscible blend, PA6/PP, the blend filled with clay, PA6/PP/C15A, and the blend with modified PP and clay, PA6/PP/PP-g-MA/C15A. The quality of the distributive mixing seems comparable, but the dispersion levels are obviously different. As represented in Figure 4b, the corresponding average diameters of the dispersed phase are 10.03 μm, 0.57 μm and 0.34 μm, respectively.

The addition of the organoclay produced a significant decrease in the size of the dispersed PP particles. In principle, this could be due to a physical interaction promoted by the presence of the high

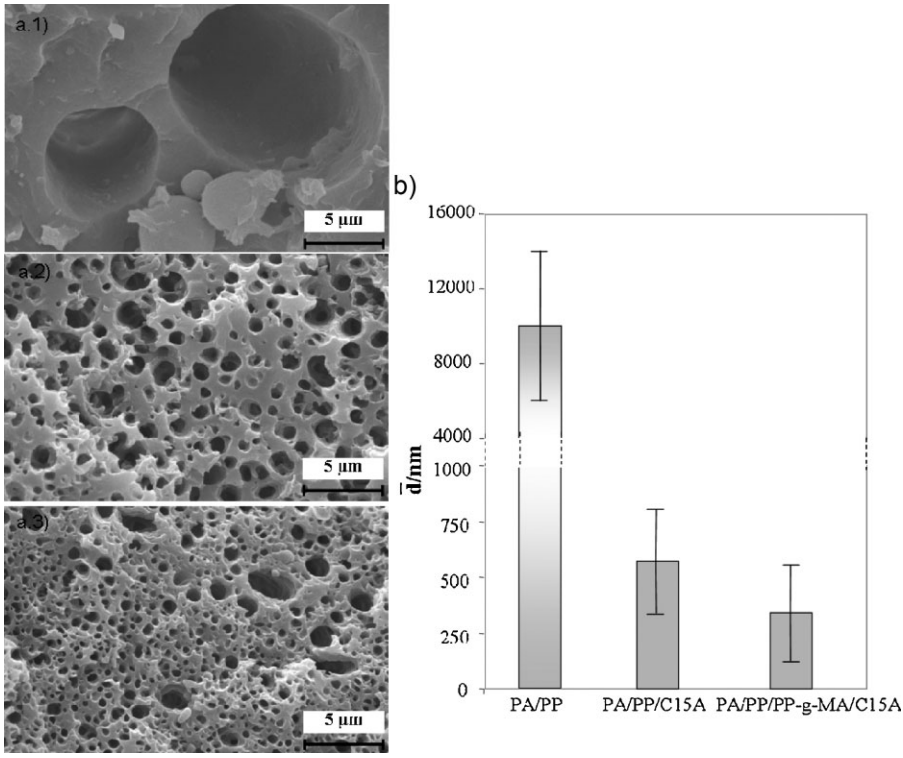

Figure 4.
Morphology (a) and average diameter of the dispersed phase (b) at the die exit, for the immiscible blend PA6/PP (a.1) and nanocomposites PA6/PP/C15A (a.2) and PA6/PP/PP-g-MA/C15A (a.3).

aspect ratio silicate nanolayers. The additional decrease brought about by the incorporation of the modified PP can be explained by the formation of a block copolymer at the interface, between the amine groups of the PA6 and the anhydride groups of the PP-g-MA.[17] Thus, these results point out that the reduction of particle size can be achieved by the addition of nanoclays and by graft copolymer formation at the interface. Within the experimental error values, the data of Figure 4b and Figure 3b correlate well, i.e., a correlation between morphology and rheological response seems to exist.

The eventual physical interaction promoted by the presence of the silicate nanolayers could consist, for example, in an adsorption process. In principle, TEM observations could test this hypothesis, as they can provide information on the location of the nanoclays in the nanocomposite. Figure 5 shows the morphologies of PA6/PP/C15A and PA6/PP/PP-g-MA/C15A at the die exit, for two different magnifications. The lighter grey areas correspond to PP and the darker areas refer to the clay. In the case of the PA6/PP/C15A nanocomposite, the silicate layers are either located at the interface, or dispersed in the PA6. Clearly, the organoclay has much more affinity with PA6 than with PP. At the highest magnification, an intercalated structure, with some degree of exfoliation, seems to be present. Here, the exfoliated nanolayers seem to produce a physical barrier between the two blend components. In case of the PA6/PP/PP-g-MA/C15A composite, the organoclay layers are mostly located at the interface between PA6 and PP. Thus, the copolymer formed improves the dispersion of the aluminosilicate layers at the interface.

Therefore, the differences in particle size of the two nanocomposites shown in Figure 4 seem to be due to the amount of organoclay located at the interface, the higher this amount, the smaller the particle size. Similar conclusions have been reported before and are usually attributed to a compatibilization effect of the simultaneous presence of PP-g-MA and organoclay.[7–11]

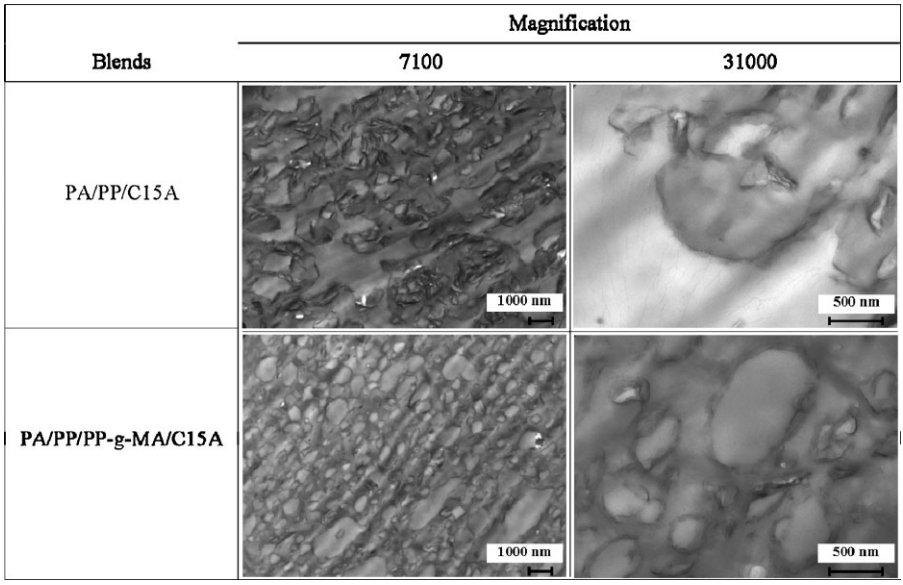

Figure 5.
TEM micrographs (magnification 7100× and 31000×) of nanocomposites PA6/PP/C15A and PA6/PP/PP-g-MA/C15A at the die exit.

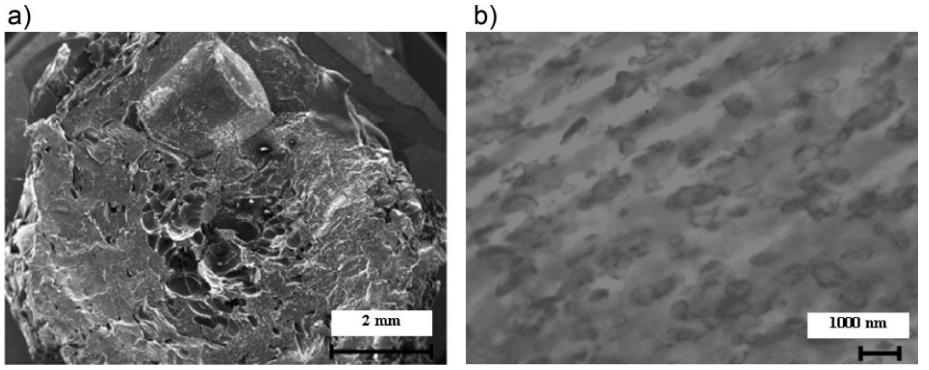

Figure 6.
Morphology of PA6/PP/PP-g-MA/C15A at L/D = 8.8. Left: SEM micrograph. Right: TEM micrograph.

Evolution Along the Screws

Since good nanoclay dispersion levels were obtained with the compounding conditions adopted, it seems interesting to investigate how dispersion evolved along the screw length. The sample collecting devices were used for this purpose, the same characterization techniques having been used.

It is interesting to note that if samples collected at L/D = 9.4 (see Figure 1) were completely molten, material at L/D = 8.8 still contained solids, as seen in Figure 6 left, where a pellet is clearly visible. However, a TEM micrograph of the melted fraction (Figure 6 right) reveals a PP matrix and a well distributed, but still relatively coarse, PA6 dispersed phase. At this stage, the clay seems to be suspended in the PA6 phase. It seems reasonable to assume that initially PP will form the matrix due to its lower melting temperature (circa 160 °C versus 220 °C); once PA6 melts, phase inversion should occur.

The X-ray spectra of the nanocomposites samples collected along the extruder are presented in Figure 7. As the material progresses along the screws, the characteristic peak of the crystalline C15A nanoclay shifts to lower angles. This corresponds to an increase in the silicate interlayer distance, i.e., the progressive formation of an intercalated structure. This process is obvious in both cases. At the die no peak can be identified, hence some exfoliated silicate layers could also have been formed simultaneously with the intercalated structures.

Figure 8 shows the evolution along the screw axis (from L/D = 9.4 onwards) of the

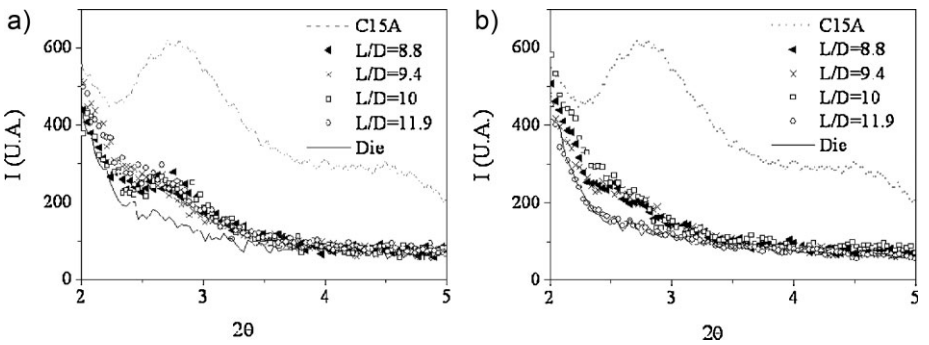

Figure 7.
X-ray diffraction spectra of samples collected along the extruder: a) PA6/PP/C15A; b) PA6/PP/PP-g-MA/C15A.

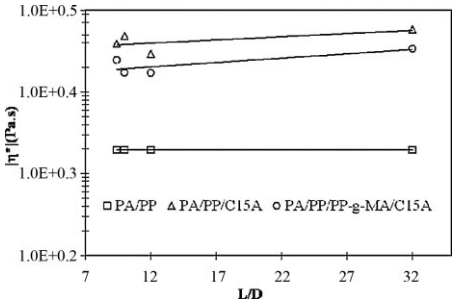

Figure 8.
Evolution along the screw of the dynamic viscosity of PA6/PP, PA6/PP/C15A and PA6/PP/PP-g-MA/C15A (at 0.07 Hz).

dynamic viscosity of the three materials under study. The viscosities of the two nanocomposites are much higher than that of the PA6/PP blend, which is to be expected and results from the decrease in size of the dispersed particles. Little evolution is seen along the extruder, which seems to indicate that most of the dispersion takes place in the initial process stages, upon melting, when high stresses, complex flow patterns and intense surface generation develop.

Figure 9 depicts the axial evolution of the morphology of the PA6/PP/PP-g-MA/C15A nanocomposite, as seen by TEM (Figure 6 right can also be used for this purpose). Phase inversion seems to occur between L/D = 8.8 and L/D = 10, due to melting of all PA6. At L/D = 10 the morphology is close to the final, at L/D = 11.9 the morphology is similar to the die exit. Flow through the various screw mixing zones will progressively improve the dispersion levels.

Conclusion

An immiscible PA6/PP 70/30 w/w blend was compatibilized with modified PP and filled with a montmorillonite-based organoclay using twin-screw melt compounding. The dispersion of the nanoclay into the polymer matrix and its eventual compatibilization effect were investigated both at the die exit and along the screw axis, by collecting samples from within the extruder at relevant locations and characterizing them by X-ray diffraction, oscillatory rheometry and SEM and TEM.

XRD and TEM data showed evidence of the presence of intercalated and exfoliated clays at the die exit. Measurements of the viscosity along the screw indicated that little evolution in morphology was probably taking place. This unexpected result was corroborated by TEM observations, that evidenced that the major steps of morphology development occur upon melting, upstream of the location where rheological measurements become possible.

Two mechanism that can reduce the particle size were identified: the location of the nanoclays at the interface and the formation of a graft copolymer.

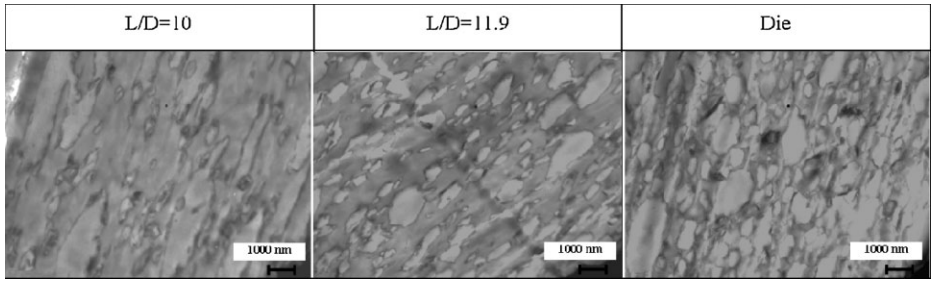

Figure 9.
TEM micrographics at high magnification (12 000×) along the extruder screw axis of the compatibilized PA6/PP/PP-g-MA/C15A at L/D = 10, 11.9 ratio and die.

[1] J. I. Weon, J. Sue, *Polymer* **2005**, *46*, 6325.
[2] N. Sheng, R. E. Cohen, *Polymer* **2004**, *45*, 487.
[3] Y. Tang, W. Fan, *Polymer* **2004**, *45*, 5317.
[4] S. S. Ray, M. Bousmina, *Macromol. Rapid Commun.* **2005**, *26*, 450.
[5] Y. Dong, D. Bhattacharyya, *Composites: Part A* **2008**, *39*, 2864.
[6] Y. Yoo, D. R. Paul, *Polymer* **2008**, *49*, 3795.
[7] G. Chen, H. Kim, E. Kim, J. Yoon, *Polymer* **2005**, *46*, 11829.
[8] S. Ray, M. Bousmina, *Polymer* **2005**, *46*, 12430.
[9] J. Hong, H. Namkung, K. Ahn, S. Lee, C. Kim, *Polymer* **2006**, *47*, 3967.
[10] B. B. Khatua, D. J. Lee, H. Y. Kim, J. K. Kim, *Macromolecules* **2004**, *37*, 2454.
[11] Y. Yoo, C. Park, S. Lee, K. Choi, D. Kim, J. Lee, *Macromolecules Chemistry Physics* **2005**, *206*, 878.
[12] D. P. Dharaiya, S. C. Jana, *J. Polym. Sci.: Part B: Polym. Phys.*, **2005**, *43*, 3638.
[13] W. Lertwimolnun, B. Vergnes, *Polym. Eng. Sci.* **2007**, *47*, 2100.
[14] W. S. Chow, Z. A. Mohd Ishak, J. Karger-Kocsis, A. A. Apostolov, U. S. Ishiaku, *Polymer* **2003**, *44*, 7427.
[15] D. W. Schaefer, R. S. Justice, *Macromolecules* **2007**, *40*, 8501.
[16] W. Lertwimolnun, B. Vergnes, *Polymer* **2005**, *46*, 3462.
[17] A. V. Machado, J. A. Covas, M. van Duin, *J. Polym. Sci.: Part A: Polym. Chem.* **1999**, *37*, 1311.

